Research on Chemical Intermediates (2021) 47:131–156
https://doi.org/10.1007/s11164-020-04330-5

Selective oxidation of aromatic alcohols in the presence of C_3N_4 photocatalysts derived from the polycondensation of melamine, cyanuric and barbituric acids

Elisa I. García-López[1] · Zahra Abbasi[2] · Francesco Di Franco[3] · Monica Santamaria[3] · Giuseppe Marcì[3] · Leonardo Palmisano[3]

Received: 8 September 2020 / Accepted: 22 September 2020 / Published online: 18 January 2021

Abstract

A set of C_3N_4 samples has been prepared by using melamine, cyanuric acid and barbituric acid as the precursors. The materials were subjected both to physical and chemical characterization and were used as photocatalysts for the selective oxidation of aromatic alcohols in water suspension under UV and visible irradiation. The photoactivity of the materials versus the partial oxidation of four substituted benzyl alcohols was investigated. The type and position of the substituents in the aromatic molecule influenced conversion and selectivity to the corresponding aldehyde. The presence of barbituric and cyanuric acids in the preparation method has changed the graphitic-C_3N_4 structure, and therefore both the characteristics of the material and the ability of light to activate the surface of the photocatalyst. The most active material prepared in the presence of melamine and cyanuric acid showed a remarkable selectivity towards the aldehyde even under visible irradiation.

Keywords Photocatalysis · Selective oxidation · C_3N_4 · Aromatic alcohol · Benzyl alcohols

✉ Elisa I. García-López
elisaisabel.garcialopez@unipa.it

[1] Department of Biological, Chemical and Pharmaceutical Sciences and Technologies, (STEBICEF), Università Di Palermo, Viale delle Scienze, 90128 Palermo, Italy

[2] Department of Chemistry, Faculty of Science, Shahid Chamran University of Ahvaz, Ahvaz, Iran

[3] Dipartimento Di Ingegneria (DI), Università Di Palermo, Viale delle Scienze, 90128 Palermo, Italy

Introduction

Heterogeneous photocatalysis is a widely applied technology to achieve the complete mineralization of pollutants. The use of TiO_2 under UV irradiation has been extensively reported to unselectively attack organic species until their mineralization to CO_2 and H_2O. However, the use of photocatalysis to obtain chemicals with high added value through oxidation or selective reduction of some substrates has recently been reported, demonstrating how this technology can be a green alternative to thermal catalysis processes [1]. In fact, compared with many catalytic oxidation reactions, no toxic by-products are generally formed, and moreover, solar radiation could be used by choosing the appropriate photocatalyst. The selective oxidation of alcohols to their corresponding aldehydes with O_2 or air is a very important chemical transformation from an industrial point of view. According to Mallat et al., benzyl alcohols can be readily transformed by heterogeneous catalysis to aldehydes that are relatively resistant to further oxidation [2]. Due to the extensive applications of benzaldehydes in pharmaceutical, fragrance and agricultural industry, many efforts have been focused on the benzyl alcohol to aldehyde photocatalytic system to obtain an efficient and low-cost system and a wide variety of photocatalysts to be used for this type of reaction [3–5]. This reaction was carried out in the presence of TiO_2-based photocatalysts [6, 7], although in most cases, organic solvents (mainly acetonitrile) were used or the liquid alcohol was directly oxidized [8, 9]. Qamar et al. used hypostoichiometric tungsten oxide (WO_{3-x}) modified with Pt and/or reduced graphene oxide (RGO) to obtain a conversion of ca. 99% with a selectivity to the aldehyde of ca. 80% under simulated sunlight and ambient conditions [10]. Also, ternary oxides, as $Bi_4O_5Br_2$, have been used for the selective photocatalytic oxidation of benzyl alcohol into benzaldehyde using acetonitrile as the solvent and a blue LED as the irradiation source. Maximum conversion of ca. 90% with 99% of selectivity was found [11].

In a photocatalytic process, when a semiconductor is irradiated by a suitable radiation, the electrons are promoted from the valence band to the conduction band. Photogenerated electrons can reduce a substrate adsorbed on the surface of the photocatalyst, which is generally oxygen if the process is performed in the air. In turn, the photoproduced holes, generated in the valence band, allow the donation of electrons from the adsorbed species, producing the oxidation reaction.

In order to increase the selectivity towards the partial oxidation products in the photocatalytic reaction, it is desirable to reduce the oxidizing capacity of the photocatalyst. This occurs by decreasing the presence of some photogenerated reactive oxygen species (ROS), i.e. hydroxyl radicals ($^{\cdot}OH$), superoxide radicals ($^{\cdot}O_2^-$), hydrogen peroxide H_2O_2 and singlet oxygen ($^1O_2$). The most popular photocatalyst, TiO_2, easily forms, under UV irradiation in an aqueous suspension, highly oxidizing $^{\cdot}OH$ species that attack non-selectively the organic molecules until they are mineralized in CO_2 and H_2O. Consequently, for selective partial oxidation purposes, the organic semiconductor polymeric carbon nitride (g-C_3N_4) appears to be a good candidate because it has insufficient potential of the low valence band to directly oxidize the water molecules to OH radicals [12].

The position of the CB edge of C_3N_4 allows the one-electron reduction of O_2 giving rise to the formation of $^{\cdot}O_2^-$ in aerated suspensions. In addition, in aqueous systems, photogenerated $^{\cdot}O_2^-/^{\cdot}O_2H$ species can be transformed into H_2O_2, which can be involved in subsequent reactions producing also $^{\cdot}OH$ [13]. Although water is considered the ideal solvent from the sustainability point of view, however, most of the selective photo-oxidation reactions are carried out in organic solvents since water does not allow an easy control of the reaction path. Antonietti et al. used for the first time the C_3N_4 polymer as a metal-free photocatalyst for the selective oxidation of benzyl alcohols in the presence of trifluorotoluene as the solvent [14]. Successive efforts have given successful results in benzyl alcohol selective oxidation by using C_3N_4 aqueous dispersions. For instance, Long et al. used a photocatalytic reactor working at 0.87 mPa of oxygen pressure and at 100 °C to obtain ca. 80% conversion of 4-methoxybenzyl alcohol with a selectivity to the corresponding aldehyde of 65% after 3 h of reaction [15]. Thermo-etched [16, 17] co-ordinated to H_2O_2 [18–20] or P-doped graphitic C_3N_4 samples [21] have been successfully used for partial photo-oxidation reactions of aromatic alcohols in aqueous suspensions obtaining selectively the corresponding aldehydes with excellent yields. Substituted benzyl alcohols have been converted to the corresponding aldehydes using carbon nitride as the photocatalyst with almost 100% selectivity [18–22], although attempts with more complex benzyl alcohols such as piperonyl alcohol have shown worse results [20, 21].

The reactivity of benzyl alcohols is drastically influenced by the number of substituents, as well as their electronic nature and the position of the substituent in the aromatic ring [23, 24]. Hammett's constants (σ) [25] were used to correlate the oxidation capacity of the aromatic species with the nature and position of the substituent. This has been reported, for example, for phenols photo-Fenton degradation [26], or the electrochemical [27] and photocatalytic oxidation of benzyl alcohols in the presence of Ru-TiO_2 [28].

An important advantage of using the C_3N_4 photocatalyst is related to the light absorption efficiency that regulates the number of active photoproduced electrons/holes. TiO_2 requires ultraviolet (UV) irradiation to induce reactions due to its relatively large band gap (about 3.2 eV), but only a low fraction (about 5%) of UV photons is present in sunlight. Consequently, the use of a photocatalyst which can be activated under visible light irradiation is of paramount importance from the practical viewpoint because visible light accounts for ~50% of the total solar energy. The band gap of the carbon nitride materials overlaps the visible light spectrum of the solar irradiation as the band gap is in the range 2.7–2.8 eV [12, 13], corresponding to ca. 450–460 nm. Furthermore, a photocatalyst having a high specific surface is particularly interesting, providing an increasing amount of active sites for the reaction. The graphitic g-C_3N_4 obtained from the calcination of melamine gives rise to a material with a low specific surface area (SSA) (about 6 $m^2\ g^{-1}$). A subsequent heat treatment of this sample provides a thermo-etched 2D exfoliated solid with a higher specific surface area which in fact shows a greater photocatalytic activity, but this powder is obtained with a low yield [16].

Some authors have reported obtaining of nanostructured g-C_3N_4 materials of well-designed composition and structure by the formation of stable

aggregates using some precursor molecules with similar structure which are able to self-assemble. This methodology is known as "supramolecular preorganization approach" [29]. The precursor molecules would form hydrogen bonding in suspension and subsequently generate stable aggregates which define the final structure of the C_3N_4. Several examples of the supramolecular preorganization methodology to obtain C_3N_4 are reported in the literature using as precursors melamine along with cyanuric acid, trithiocyanuric acid, barbituric acid, 2,4,6-triaminopyrimidine, among others, resulting in the development of different surface morphologies and features of C_3N_4. Also, the introduction of functional groups on the g-C_3N_4 surface by the use of these precursors can increase the SSA and therefore the number of active sites thus improving the adsorption of the substrate [30–32]. These functional groups can play different roles on the material. For example, according to Tan et al., g-C_3N_4 rich in cyano groups, prepared by adding cyanuric acid to melamine during the preparation of the photocatalyst, showed an increase in the degradation of benzylamine [33]. The cyano group in the g-C_3N_4 framework is responsible for improving the adsorption of O_2 by causing the electrons of the solitary pair in the structure to be continuously involved in the photo-excitation process. The polarization of the cyano groups also improves the adsorption capacity of the solid, and therefore generally the photocatalytic activity, even if there is no direct correlation between adsorption and photoactivity.

Shalom et al. [34] also prepared a C_3N_4 structure using a mixture of cyanuric acid-melamine as the starting precursor. They added barbituric acid (BA) which led to an increase in optical density along with a shift towards red in the light absorption of the semiconductor prepared [35, 36].

Antonietti et al. obtained the thermal polycondensation of barbituric acid only, as a monomeric precursor to give the final polymeric semiconductor. The authors claim to obtain excellent absorption of visible light thanks to the presence of a conjugated system highly polarizable in the structure. The material exhibited photocatalytic activity for the bleaching of RhB in aqueous solution. RhB photocatalytic bleaching was attributed to the direct photo-oxidation of the strongly adsorbed dye by the photogenerated holes of the solid photocatalyst [37].

In the present research, some materials based on the organic 2D semiconductor polymer C_3N_4 have been prepared using melamine as the precursor in the presence of cyanuric and barbituric acids. The semiconductors obtained were subjected both to physical and chemical characterization, and they have been used as photocatalysts for the selective partial photo-oxidation of alcohols to the corresponding aldehydes in water suspension at room conditions. The aromatic alcohols used as the substrates were benzyl alcohol and some derivatives having a substituent in the *para*-position (4-methoxy, 4-nitro and 4-hydroxy). Notably, the aldehydes obtained from the partial photo-oxidation of the alcohols are important intermediates for the synthesis of fine chemicals, as for instance pharmaceuticals and agricultural chemicals. The alcohols were chosen by taking into account that the presence of different substituents on the aromatic ring can influence in a different way both the conversion and the selectivity.

Experimental

Preparation of the photocatalysts

Melamine, cyanuric acid and barbituric acid (Sigma-Aldrich, analysis grade) have been used as precursors for the g-C_3N_4 preparation. A first sample was prepared by dissolving 5.1 g of cyanuric acid (Cy) in 100 mL of water and by slowly adding 5 g of melamine (molar ratio 1:1). The resulting white suspension was stirred for 1 h and heated at ca. 50 °C until complete dryness. The white powder was then calcined in a closed ceramic crucible up to 520 °C (2 °C min^{-1}) and left for 2 h at 520 °C. After calcination, the resulting white powder was labelled as C_3N_4-Cy 1-1-0.

Three further materials were prepared by using the initial cyanuric acid (Cy) solution which contained also a certain amount of barbituric acid (B) that was completely soluble. The melamine was added to the solution containing both cyanuric and barbituric acids. Molar ratios of cyanuric acid/barbituric acid 1:0.2; 1:0.5 and 1:1 were used in these solutions. 5 g of melamine was added to each solution, and after 1 h of stirring, the suspension was heated at 50 °C to dryness. Subsequently, each white powder was calcined at 520 °C, as previously described. The colour of the samples changed from yellow to orange and brown and became darker after the calcination procedure increasing the quantity of barbituric acid. The powders were labelled as C_3N_4-Cy-B 1-1-0.2; 1-1-0.5 and 1-1-1. The numbers in the labels of the samples are related to the molar ratios of melamine-cyanuric acid-barbituric acid in the samples. Also, a material prepared by using only melamine, labelled as g-C_3N_4, was prepared for the sake of comparison. It was obtained following the method previously described [16]. In brief, 10 g of melamine was placed in a covered ceramic crucible, heated at 520 °C (2 °C min^{-1}) and left for 2 h. The strongly coloured aspect of the samples containing barbituric acid reported in Fig. 1a is very similar to that of the materials obtained by Antonietti et al. [37] who used only barbituric acid as precursor of the C_3N_4.

Physicochemical characterization of the materials

XRD patterns were obtained with an X-ray diffractometer (PANanalytical Empyrean), equipped with a Cu anode (Kα radiation, $\lambda = 0.15405$ nm, operating voltage: 40 kV, operating current: 40 mA). Scanning electron microscopy (SEM) observations were performed on the samples after deposition by sputtering of a thin gold layer, using an FEI Quanta 200 SEM microscope operating in high vacuum at 30 kV. Infrared spectra of the samples in KBr (Aldrich) pellets were recorded with 4 cm^{-1} resolution and 256 scans using an FTIR-8400 Shimadzu spectrometer. Diffuse reflectance spectra (DRS) were obtained in air at room temperature in the 250−800 nm wavelengths range by means of a Shimadzu UV-2401 PC spectrophotometer, with $BaSO_4$ as the reference material. Mixtures of the photocatalysts with $BaSO_4$ in a mass ratio 0.050:1 were used.

A photoelectrochemical characterization was performed to study generation and transport of photoexcited charge carriers in the photocatalysts, obtaining information

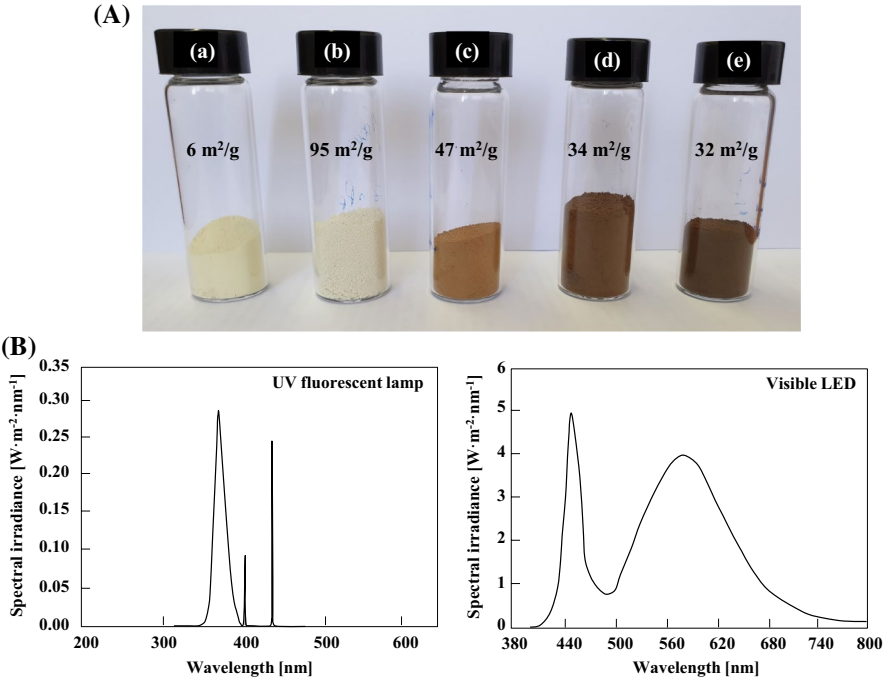

Fig. 1 **A** Picture of the photocatalysts: **a** g-C_3N_4; **b** C_3N_4-Cy 1-1-0; **c** C_3N_4-Cy-B 1-1-0.2; **d** C_3N_4-Cy-B 1-1-0.5 and **e** C_3N_4-Cy-B 1–1-1 and **B** spectral irradiance of the irradiation sources used for the photocatalytic experiments

on their electronic properties such as band gap, flat band potential and photoactivity. The photoelectrochemical characterization was carried out by using a 450 W UV–Vis Xenon lamp coupled with a Kratos monochromator, which allowed a monochromatic irradiation of the specimen filtered through a quartz window present in the cell. A two-phase lock-in amplifier was used, coupled with a mechanical chopper (frequency of 13 Hz), allowing to extract photocurrent signals from the total current circulating in the cell. To estimate the optical band gap, photocurrent spectra were corrected for the relative photon flux of the light source at each wavelength. All the photoelectrochemical measurements were carried out in 0.1 M ammonium biborate tetrahydrate electrolyte (ABE, $(NH_4)_2B_4O_7{\cdot}4H_2O$; pH ~ 9) at room temperature (RT) with a three-electrode configuration using a Pt wire as counter electrode and Ag/AgCl/sat. KCl electrode (0 V vs. Ag/AgCl = 0.197 V vs. SHE) as the reference electrode. For these measurements, different C_3N_4 photocatalysts were deposited on carbon paper (Toray 40% wet Proofed-E-Tek).

Photocatalytic activity under UV or visible irradiation

The partial oxidation of four aromatic alcohols, i.e. benzyl alcohol (BA), 4-methoxybenzyl alcohol (4-MBA) 4-nitrobenzyl alcohol (4-NBA) and 4-hydroxybenzyl

alcohol (4-OHBA) to their corresponding aldehydes, i.e. benzaldehyde (BAL), 4-methoxy benzaldehyde (4-MBAL), 4-nitrobenzaldehyde (4-NBAL) and 4-hydoxy-benzaldehyde (4-OHBAL), respectively, was studied.

The photocatalytic experiments were carried out by using two different set-ups. In the first one, 150 mL of aqueous suspension was placed in a Pyrex cylindrical photoreactor externally irradiated by six Actinic BL TL MINI 15 W/10 Philips fluorescent lamps emitting in the 340–420 nm wavelength range (main emission peak at 365 nm) (See Fig. 1b). The lamps were fitted at 3 cm distance from the reactor axis. The photon flux reaching the external wall of the photoreactor was measured by a radiometer Delta Ohm DO9721 with a UVA probe in the range 315–400 nm and it resulted ca. 8 W m^{-2}. The emission in 450–900 nm range was null. The photoreactor was equipped by a thimble with circulating water that allowed to keep the temperature of the suspension at ca. 25 °C.

The second set-up consisted of a cylindrical Pyrex batch photoreactor of 150 mL externally surrounded co-axially by a 120 W visible LED strip. The average photon flux impinging the reactor was ca. 800 W m^{-2} in the 450–950 nm range. The LED emission in the 315–400 nm range was null (See Fig. 1b). A rotor fun was used to avoid any warming up of the system which worked at room conditions.

In both set-ups, the amount of solid in suspension (0.33 g L^{-1}) was enough to absorb all the photons emitted by the irradiation source. All the experiments were carried at room temperature. Before starting the irradiation, the catalyst was added to the solution and the obtained suspension was kept in an ultrasonic bath for 10 min and eventually stirred under dark for 30 min to attain the adsorption equilibrium. During the experiments, the photoreactors were open, and the equilibrium between dissolved O_2 in the aqueous suspension and in the atmosphere was achieved. Throughout the reaction, samples of the irradiated suspension were withdrawn every 30 min and filtered through 0.25 μm membranes (HA, Millipore) to separate the photocatalyst particles before the HPLC analyses.

A Beckman Coulter HPLC apparatus equipped with a Diode Array detector was used to identify and determine the concentration of the aromatic substrates and their intermediates. A Phenomenex KINETEK 5 μm C18 column was used, and the eluent (0.8 mL min^{-1}) consisted of a mixture of acetonitrile and 13 mM trifluoroacetic acid (20:80 v:v). Standards purchased from Sigma-Aldrich with a purity > 99% were used to identify the products and to obtain the calibration curves.

Results and discussion

Characterization of the photocatalysts

The crystallinity and the layered-stacking mode of the C_3N_4-based photocatalysts were analysed by XRD. As shown in Fig. 2, the two main diffraction peaks at 13.2° and 27.6° corresponding to the (100) and (002) crystal layers of g-C_3N_4 are clearly identifiable. The (100) diffraction peak demonstrates the presence of an in-plane structural packing motif, whereas the (002) diffraction peak is attributed to the interlayer stacking of aromatic segments [38, 39]. These two diffraction peaks

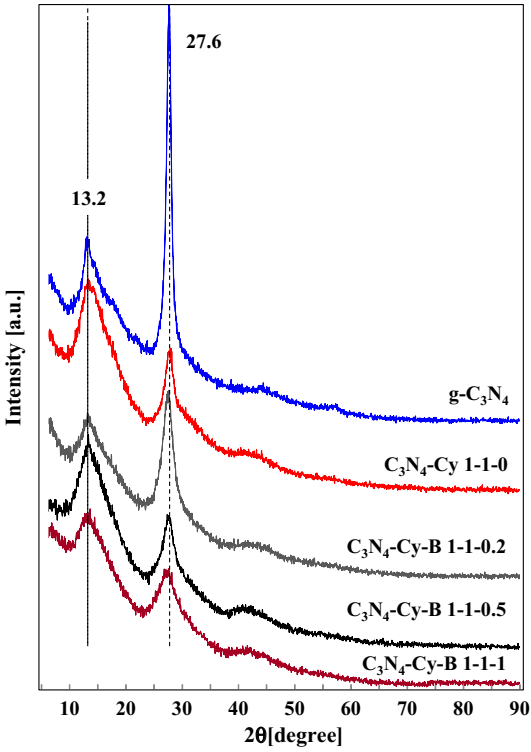

Fig. 2 XRD patterns of all the home-prepared C_3N_4-based materials

are in suitable agreement with the reported literature (JCPDS 87-1526). The results confirmed the g-C_3N_4 presence in all of the materials. There is an evident widening of the two peaks suggesting the decreasing in the periodicity and crystallinity of the samples by increasing the amount of Cy and barbituric acid (B) compared with the bare g-C_3N_4. The position of the peak at 27.6° assigned to (002) plane barely changes for the materials containing Cy and B, indicating that the interplanar distance in the carbon nitride samples is not affected with respect to g-C_3N_4. This is in accordance with previous studies [35, 38]. The widening of the characteristic diffraction peak at 13.2°, corresponding to the in-plane structural packing motif [40], indicates that the in-plane repeating heptazine units have lost symmetry by the introduction of Cy and particularly by increasing the B amount.

The surface morphology structure of the powders was examined by SEM. Figure 3A and B shows the SEM images of all the samples prepared at two different magnifications. As presented in Fig. 3A, the g-C_3N_4 sample exhibits a typical bulk-like morphology appearing as rather compact agglomerates of carbon nitride foils that give the impression as scales protruding from the material. This particular aspect can justify its low specific surface area value. On the contrary, the morphology of the C_3N_4-Cy 1-1-0 photocatalyst is completely different. A planar and layered structures are visible. The material consists of thin sheets of carbon nitride that are partially twisted on themselves. The completely exfoliated morphology of this material, due to the presence of cyanuric acid during the preparation, can also justify

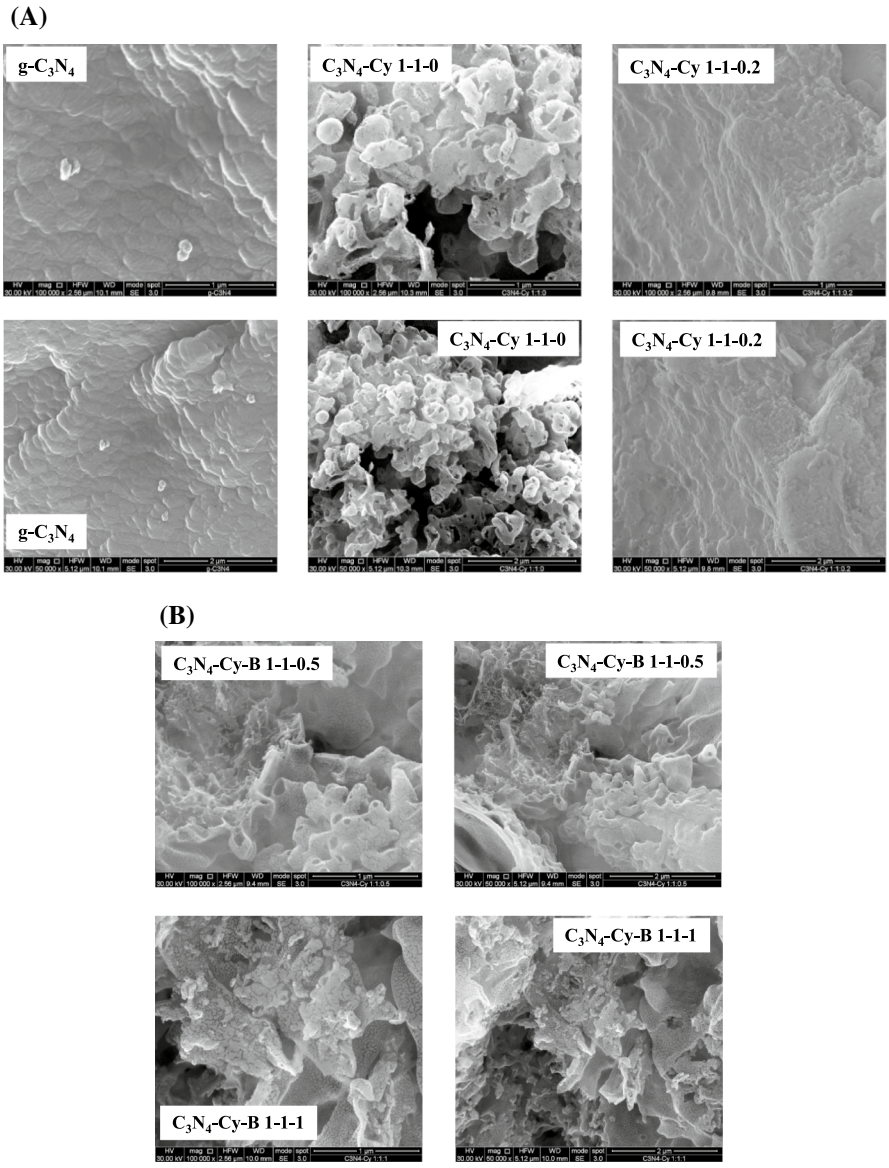

Fig. 3 SEM micrographs of the C_3N_4-based materials at two different magnifications

its higher specific surface area compared with all of the other solids. The addition of small amounts of barbituric acid causes the C_3N_4-Cy-B 1-1-0.2 appearance to be similar to the bare g-C_3N_4 sample although the carbon nitride foils appear thinner compared with those of the pristine material. Figure 3B shows that in the case of C_3N_4-Cy-B 1-1-0.5 and C_3N_4-Cy-B 1-1-1, obtained in the presence of increasing amounts of barbituric acid, the laminated graphitic structure disappeared. In

particular, in the surface of the C_3N_4-Cy-B 1-1-0.5 particles, structures similar to craters of volcanoes are visible. Those structures disappeared in the C_3N_4-Cy-B 1-1-1 material, probably because they collapsed due to the large amount of barbituric acid.

The relatively low specific surface area (SSA) of the g-C_3N_4 obtained using melamine as the precursor (in the range 4–7 $m^2\ g^{-1}$) has been reported before by us, while values close to 70 $m^2\ g^{-1}$ could be obtained by performing a post-synthetic exfoliation procedure [16]. The SSAs of the C_3N_4-based materials obtained in this research are reported in Fig. 1a. The carbon nitride prepared from the melamine-cyanuric acid complex possesses an SSA significantly higher with respect to those of the other samples, including bare g-C_3N_4 and close to the value obtained for the thermally etched C_3N_4 [16, 21]. The introduction of cyanuric acid in the g-C_3N_4 structure, according to the literature, would provide more active sites for the photocatalytic reaction. In the presence of B, the SSA of the material decreases as shown in Fig. 1a, although the values of SSA for the samples prepared by using B are higher than that of the bare g-C_3N_4.

The FTIR spectra of all of the solids are reported in Fig. 4. In general, the spectra confirmed the C_3N_4 structure of the materials, showing significant differences among the samples. The strong absorption bands in the range 1650–1200 cm^{-1}, shown in Fig. 4A, are typical stretching vibrations modes of the heptazine heterocyclic ring (C_6N_7) units [41, 42]. In particular, the absorption band at 1640 cm^{-1} can be attributed to C–N stretching, while those at 1560 cm^{-1} and in the range 1200 to 1350 cm^{-1} are the typical stretching vibration modes of C–N heterocycles [41–45]. The bands at 1315 cm^{-1} and 1238 cm^{-1} are due to the stretching vibration of C-NH-C units. Khabashesku et al. assign also the transitions located at 1460, 1407 and 1560 cm^{-1} to the double semicircle stretchings of s-triazine cycles along with that at 810 cm^{-1} due to the out-of-plane ring bending by the basic structural units of the tri-s-triazine [41, 42]. The transitions attributed to stretching and bending of the s-triazine cycles are becoming wider and also are shifted by the addition of cyanuric acid and particularly barbituric acid in the preparation of the samples. By increasing the amount of these additives, the widening and shifting of the signal increase, indicating that the local heptazine structure of the synthesized g-C_3N_4 is being distorted in the samples by the addition of cyanuric acid and barbituric acid. Indeed, the band located at 810 cm^{-1} is present in all of the powders but in C_3N_4-Cy-B 1-1-1 sample, it is particularly wider and shifted indicating a compromise of the heptazine structure. The same result is confirmed by the widening of the bands at 1407, 1460 and 1560 cm^{-1} which disappear as the amount of barbituric acid increases. Indeed, they are absent in the C_3N_4-Cy-B 1-1-1 FTIR spectra.

The vibrational transition observed at ca. 890 cm^{-1} has been assigned to a pattern of cross-linked heptazine deformation [46]. Also, the 890 cm^{-1} vibrational transition band disappeared for C_3N_4-Cy-B 1-1-0.5 and C_3N_4-Cy-B 1-1-1. Tang et al. observed a similar behaviour, i.e. the gradual weakening of the bands assigned to the structure of heptazine by the introduction of 2,4,6-triaminopyrimidine, and according to the AA, this result was due to the modification of the structure where tri-s-triazine basic units became disordered and irregular [47].

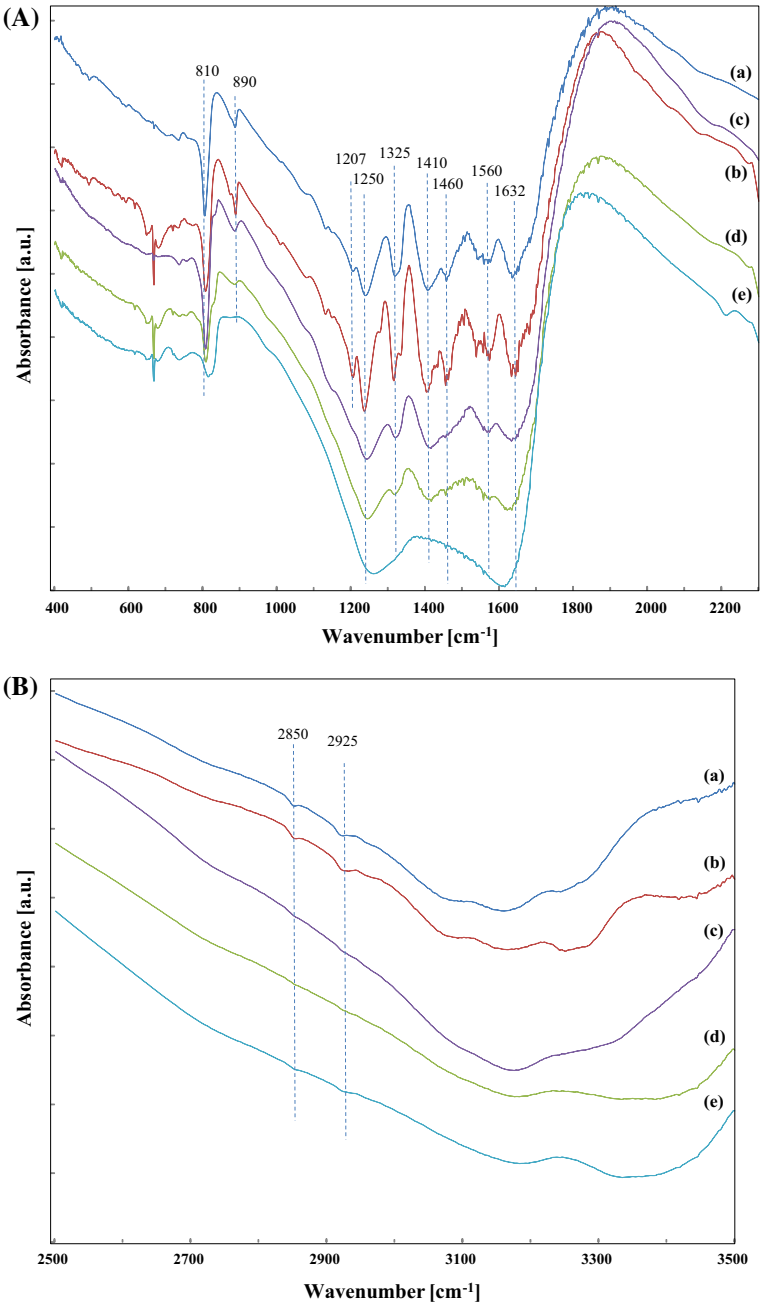

Fig. 4 FTIR spectra of the photocatalysts: **a** g-C_3N_4; **b** C_3N_4-Cy 1-1-0; **c** C_3N_4-Cy-B 1-1-0.2; **d** C_3N_4-Cy-B 1-1-0.5 and **e** C_3N_4-Cy-B 1-1-1

Figure 4B shows the broad group of peaks ranging from 3500 to 3000 cm^{-1} which can be attributed to O–H and N–H stretching, due to the presence of hydroxyl-adsorbed species and free amino groups on the surface [48–50]. The broad peak reported from 3000 to 3500 cm^{-1} contributed by the N–H stretching confirms the existence of NH and/or NH_2 groups on the surface caused by incomplete polycondensation of the C_3N_4. The cyanuric acid presence does not seem to promote further polycondensation of g-C_3N_4, indeed the spectra recorded were similar.

As shown in Fig. 4A, by increasing the amount of barbituric acid in the preparation of the photocatalyst, the IR transitions attributed to the heptazine heterocyclic ring are increasingly less defined, and for the C_3N_4-B 1-1-1 showed just wide band transitions indicative of a very disordered structure.

In Fig. 4B, the wide band appears even wider and low defined for the C_3N_4-Cy-B 1-1-0.2 sample and furtherly wide and also shifted to 3400 cm^{-1} for C_3N_4-Cy-B 1-1-0.5 and C_3N_4-Cy-B 1-1-1 samples. These findings could be explained by the loss in geometry and order of the graphitic structure motifs in the layered structure due to the presence of the barbituric acid during the samples preparation.

The optical absorptions of the polymers have been investigated by means of UV–Vis diffuse reflectance spectra (DRS). In Fig. 5, the samples show the typical broad absorption band which can be ascribed to the charge transfer process responsible for the intrinsic indirect band gap of g-C_3N_4 [51]. An evident red-shift absorption edge was observed in the presence of barbituric acid. The presence of barbituric acid during the preparation of the C_3N_4 materials could afford absorbance in the visible region, so that both UV and visible radiation can contribute to the photoactivity of the powders. It was not possible to estimate the optical band gap, E_{gap} for the samples containing barbituric acid due to the large absorption in the visible region, as shown in Fig. 5. However, it is worth mentioning that good absorbance in the visible region does not provide any guarantee for better photocatalytic activity in the event of visible irradiation. To determine the optical band gap energies of the samples which do not contain barbituric acid, the Kubelka–Munk function $F(R_\infty)$ of the

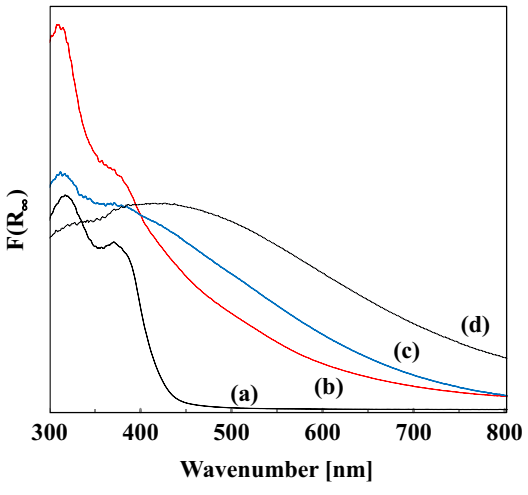

Fig. 5 Absorbance of the samples **a** C_3N_4-Cy 1-1-0; **b** C_3N_4-Cy-B 1-1-0.2; **c** C_3N_4-Cy-B 1-1-0.5 and **d** C_3N_4-Cy-B 1-1-1

DRS corresponding to the absorbance, reported in Fig. 5, has been used. The band gap values, obtained by extrapolating a linear fitting in the Tauc plot [52], i.e. the plot of $(F(R_\infty)\cdot h\nu)^{1/2}$ versus incident light energy in eV by considering the powders as indirect semiconductors were 2.70 and 2.83 eV, for g-C_3N_4 and C_3N_4-Cy 1-1-0, respectively. These values are in agreement with the colour of the materials, shown in Fig. 1A, yellow for g-C_3N_4 and pale yellow for C_3N_4-Cy 1-1-0.

In order to study the electronic properties (band gap, flat band potential and conductivity type) of the different photocatalysts, photoelectrochemical measurements were carried out. The photocurrent spectra recorded in 0.1 M ABE at the electrode potential $U_E = 1$ V versus Ag/AgCl are reported in Fig. 6A. The measured photocurrent is inversely proportional to the barbituric acid amount used to prepare the photocatalysts. Notably, for C_3N_4-Cy 1-1-0 and C_3N_4-Cy-B 1-1-0.2, a photocurrent tail was also recorded for $\lambda \geq 400$ nm using a 400 nm cut off filter. By assuming non-direct optical transitions, it is possible to estimate the band gap values according to the following equation:

$$(Q_{ph}h\nu)^{0.5}\alpha(h\nu - E_g) \quad (1)$$

where for photon energy in the vicinity of band gap, Q_{ph}, the photocurrent yield (i.e. the photocurrent corrected for the efficiency of the lamp monochomator system) is proportional to the light absorption coefficient, $h\nu$ is the photon energy and E_g is the optical band gap [53]. As shown in Fig. 6B, C, D and E by extrapolating to zero the $(Q_{ph}\ h\nu)^{0.5}$ versus $h\nu$ plots, the optical band gap values of all the

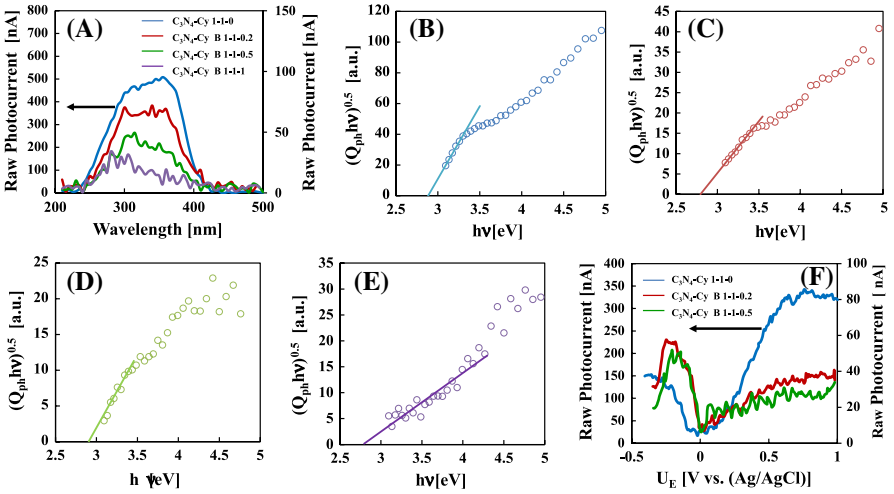

Fig. 6 **A** Raw photocurrent spectra related to different photocatalysts by polarizing samples in 0.1 M ABE solution (pH ~ 9) at $U_E = 1$ V versus Ag/AgCl. $(Q_{ph}h\nu)^{0.5}$ versus $h\nu$ plots relating to photocurrent spectra for **B** C_3N_4-Cy 1-1-0; **C** C_3N_4-Cy-B 1-1-0.2; **D** C_3N_4-Cy-B 1-1-0.5 and **E** C_3N_4-Cy-B 1-1-1. **F** Photocurrent versus U_E curves relating to different photocatalysts by scanning the electrode potential at 10 mV s^{-1} under monochromatic irradiation (350 nm, i.e. 3.5 eV) in 0.1 M ABE solution (pH ~ 9)

photocatalysts were estimated. For C_3N_4-Cy 1-1-0, a band gap of 2.85 eV was estimated, slightly lower than that estimated before for the g-C_3N_4, equal to 2.95 eV [54]. The E_g value decreases down to 2.75 eV for C_3N_4-Cy-B photocatalysts (see Fig. 6C, D and E), thus the incorporation of barbituric acid induces a red-shift of the light absorption threshold of C_3N_4. However, the disorder induced by the barbituric acid into the structure, as also confirmed by XRD and FTIR, gives rise to the formation of a defective phase causing a reduction of the photocarriers separation efficiency accounting for the very poor photocatalytic performance of the C_3N_4-Cy-B 1-1-1 material.

Raw photocurrent (I_{ph}) vs. electrode potential curves recorded under constant photon energy ($\lambda = 350$ nm, i.e. 3.5 eV) for the investigated photocatalysts are reported in Fig. 6F. There is a clear inversion of the photocurrent sign on going from anodic to cathodic polarization. The inversion photocurrent potential can be assumed as a rough estimation of the flat band potential, necessary to locate the Fermi level of the materials. According to Fig. 6F, a flat band potential of ~ 0 V versus Ag/AgCl can be estimated for all the photocatalysts. Notably, it was not possible to record I_{ph} versus electrode potential curve for C_3N_4-Cy-B 1-1-1 due to the low photoresponse in agreement with its defective structure.

Photocatalytic activity

Preliminary experiments carried out under the same experimental conditions, but in the absence of light, evidenced a modest adsorption of the aromatic substrates. The adsorption degree was less than 3% for all of the substrates on all of the solids after 30 min of stirring. No reaction product was found. It is reported that the addition of cyanuric acid along with melamine during the preparation of the photocatalyst could effectively improve the adsorption ability of the composites. This can be attributed, also in accordance with the literature, to the presence of a high porosity and to a large number of reactive sites which increase the specific surface area of the solid compared with g-C_3N_4, thus improving both the adsorption capacity and the photocatalytic performance [55]. The adsorption ability in the dark of the Cy- and B-modified C_3N_4 materials prepared in this research did not enhance with respect to the g-C_3N_4 powder, at least in our experimental conditions.

The trend of the concentration of the four model benzyl alcohols oxidation in the presence of the various photocatalysts versus the irradiation time under UV light is reported in Fig. 7. The BA substrate concentration decreased in the presence of the C_3N_4-Cy-1-1-0 sample, on the contrary, the other materials showed a low photocatalytic activity. When the photocatalysts were used for the 4-MBA oxidation, the activities were higher than by using BA as the model molecule, i.e. 4-MBA was more easily oxidized than BA. The C_3N_4-Cy 1-1-0 sample completely oxidized 4-MBA already after 90 min and the order of activity of the photocatalysts was C_3N_4-Cy 1-1-0 > C_3N_4-Cy-B 1-1-0.2 > g-C_3N_4 > C_3N_4-Cy-B 1-1-0.5 > C_3N_4-Cy-B 1-1-1. As observed for BA, the C_3N_4-Cy-B 1-1-1 sample was nearly inactive. The most recalcitrant molecules to the oxidation were 4-OHBA and 4-NBA. In both

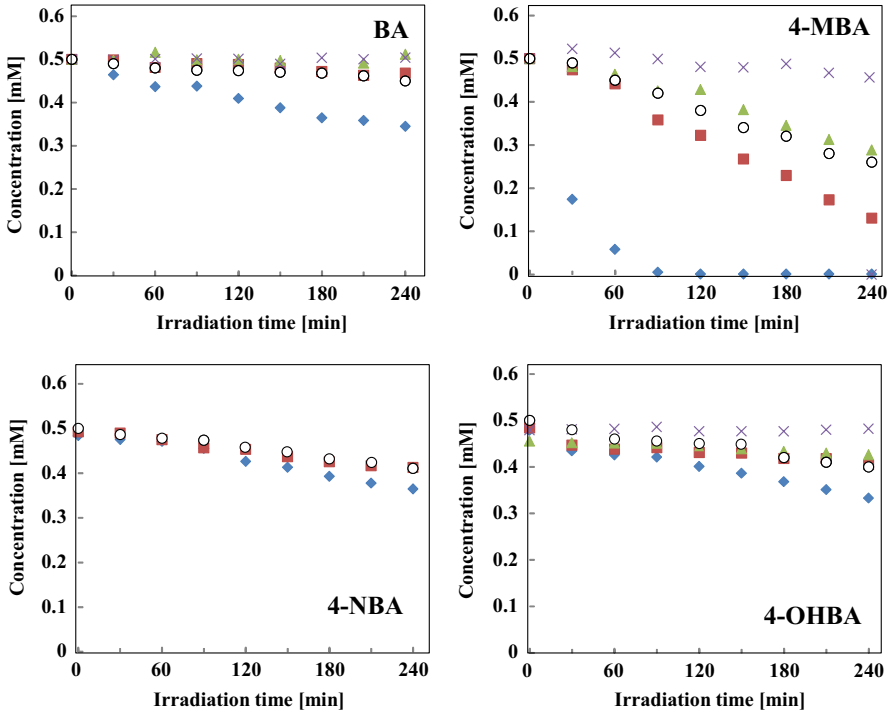

Fig. 7 Evolution of the different benzyl alcohols concentration in the presence of g-C_3N_4 (o); C_3N_4-Cy 1-1-0 (◆); C_3N_4-Cy-B 1-1-0.2 (■); C_3N_4-Cy-B 1-1-0.5 (▲); and C_3N_4-Cy-B 1-1-1 (x) vs. irradiation time by using the system provided with UV lamps

cases, the oxidation of the substrates was very modest even by using the most active sample, i.e. C_3N_4-Cy 1-1-0, which was observed to be, also for these two alcohols, the most active photocatalyst.

The photocatalytic oxidation of the benzyl alcohols gave rise merely to the corresponding aldehyde which was, after 4 h of reaction, the only product observed. Only in the case of the most active material, i.e. C_3N_4-Cy-B 1-1-0, traces of the corresponding benzoic acid species were analysed during the oxidation of 4-MBA after 120 min of UV or 210 min of visible light irradiation. In any case, the reaction was very selective to the aldehyde production. The evolution of the aldehydes' concentration corresponding to the runs reported in Fig. 7 is shown in Fig. 8.

The trend of the concentration of the four model alcohols oxidation in the presence of the various photocatalysts versus the irradiation time under visible light is reported in Fig. 9.

The concentration of the BA substrate slightly decreased in the presence of all photocatalysts, although a low activity was observed in the following decreasing order for the samples C_3N_4-Cy 1-1-0, C_3N_4-Cy-B 1-1-0.2 and g-C_3N_4. Notably, the activity was instead remarkable for 4-MBA, and even under visible

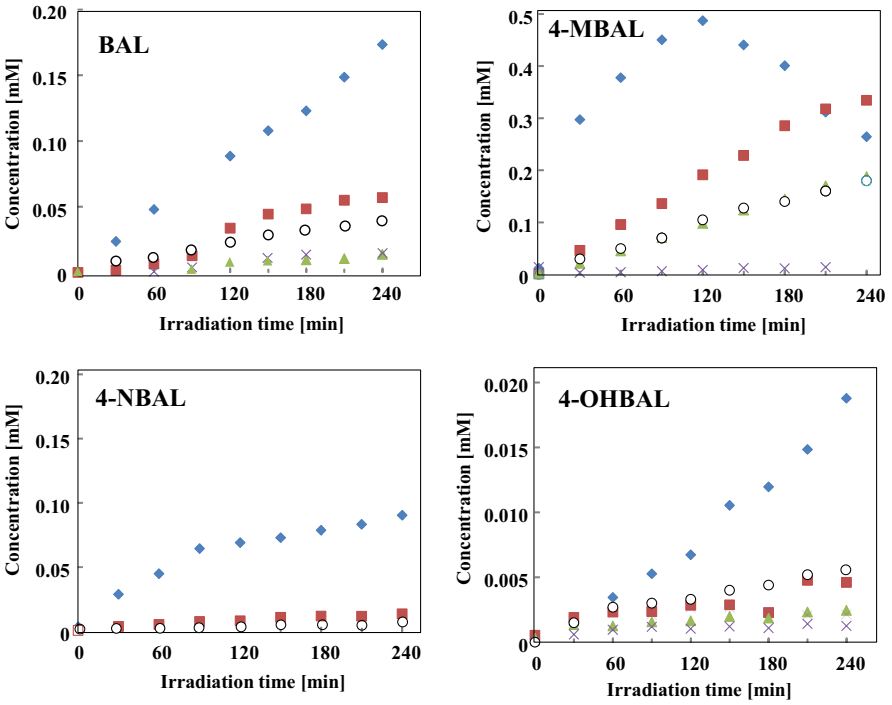

Fig. 8 Evolution of the concentration of benzaldehydes formed in the presence of g-C_3N_4 (o); C_3N_4-Cy 1-1-0 (♦); C_3N_4-Cy-B 1-1-0.2 (■); C_3N_4-Cy-B 1-1-0.5 (▲); and C_3N_4-Cy-B 1-1-1 (**x**) vs. irradiation time by using the system provided with UV lamps

light, this substrate was the easiest to partially oxidize, being also in this case the C_3N_4-Cy-1-1-0 sample the most active, followed by C_3N_4-Cy-B 1-1-0.2 and g-C_3N_4. 4-MBA was completely oxidized after ca. 210 min in the presence of C_3N_4-Cy 1-1-0. 4-OHBA was very moderately oxidized in the presence of all of the photocatalysts. For each aromatic alcohol, the order of activity of the set of photocatalysts is the same obtained under UV irradiation: C_3N_4-Cy 1-1-0 > C_3N_4-Cy-B 1-1-0.2 > g-C_3N_4 > C_3N_4-Cy-B 1-1-0.5 > C_3N_4-Cy-B 1-1-1. The most recalcitrant substrate to be oxidized was 4-NBA, and it was more difficult to be partially oxidized even by using the most active photocatalyst, i.e. C_3N_4-Cy 1-1-0.

The only products obtained during the irradiation of benzyl alcohols under visible light were the corresponding benzaldehydes. The evolution of the benzaldehydes concentration during the experiments carried out under visible light irradiation is reported in Fig. 10. Notably, 4-MBAL was obtained quantitatively (100% selectivity) after 210 min of irradiation, a time at which the conversion of 4-MBA was also 100%.

The conversion of the alcohol (X) and the selectivity of the reaction to the corresponding aldehyde (S) during the photocatalytic experiments were calculated as follows:

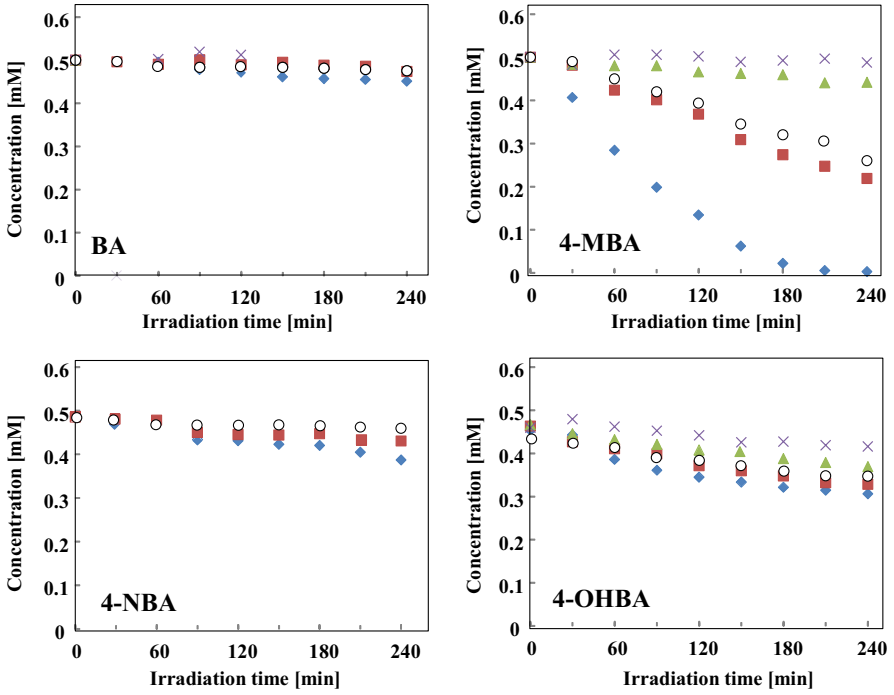

Fig. 9 Evolution of the different benzyl alcohols concentration in the presence of g-C_3N_4 (o); C_3N_4-Cy 1-1-0 (♦); C_3N_4-Cy-B 1-1-0.2 (■); C_3N_4-Cy-B 1-1-0.5 (▲); and C_3N_4-Cy-B 1-1-1 (x) vs. irradiation time by using the system provided with a visible LED

$$X = \left([\text{alcohol}]_{\text{initial}} - [\text{alcohol}]\right) / [\text{alcohol}]_{\text{initial}} \times 100 \quad (2)$$

$$S = [\text{aldehyde}] / \left([\text{alcohol}]_{\text{initial}} - [\text{alcohol}]\right) \times 100 \quad (3)$$

In any case, the aldehyde was the only product analysed in the reagent suspension. Small amounts of aldehyde-derived acid species were found only in the presence of the most active photocatalyst C_3N_4-Cy 1-1-0, during the oxidation of 4-MBA after 120 min of UV or 210 min of visible light irradiation. Benzyl alcohol conversion and selectivity towards aldehydes after 4 h of reaction in the presence of the various photocatalysts under UV radiation are reported in Table 1. Each of the figures reported in Table 1 was obtained using the average value of two experiments and the error is approx. 1–2%.

The perusal of Table 1 shows that, generally, as far as the conversion is concerned, the most active photocatalyst was C_3N_4-Cy 1-1-0 in any condition and for all substrates. It is worth noting that this material also has the highest specific surface area. By considering the results obtained under UV light irradiation, C_3N_4-Cy 1-1-0 gave rise to the highest conversion with respect to the other photocatalysts. Indeed, it reached a 100% conversion of 4-MBA, and in this experiment, the selectivity was also 100% after 120 min under UV or after 210 min under visible light irradiation.

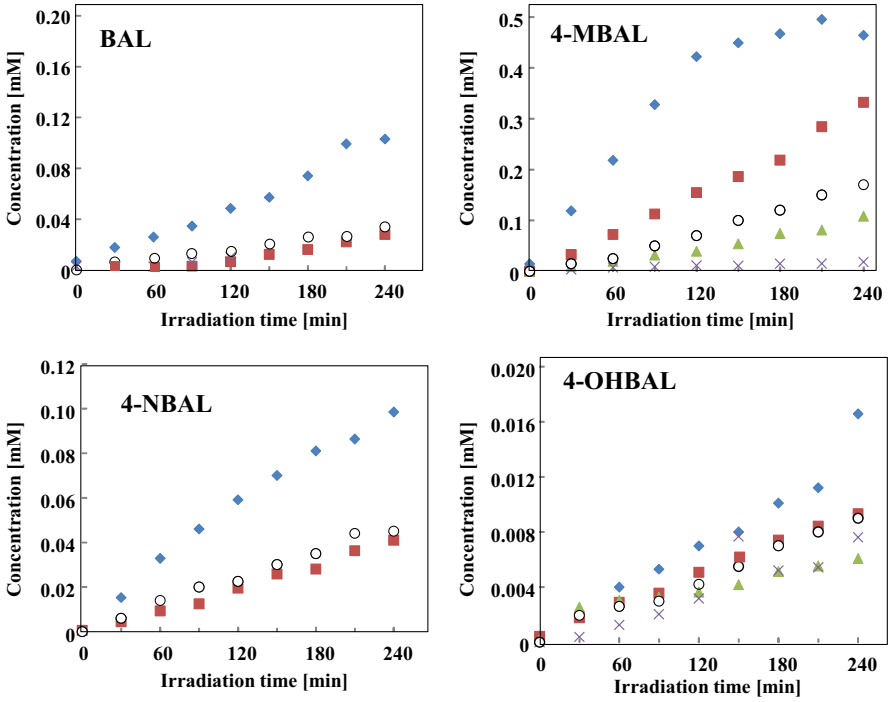

Fig. 10 Evolution of the concentration of benzaldehydes formed in the presence of g-C_3N_4 (o); C_3N_4-Cy 1-1-0 (♦); C_3N_4-Cy-B 1-1-0.2 (■); C_3N_4-Cy-B 1-1-0.5 (▲); and C_3N_4-Cy-B 1-1-1 (**x**) vs. irradiation time by using the system provided with a visible LED

The selectivity figures in Table 1 for 4-MBAL are lower than 100% due to the overoxidation of the aldehyde by continuing the irradiation of the system, as shown in Figs. 8, 10 in which the concentration of 4-MBAL first increases and then, after reaching a maximum, decreases. In these runs also benzoic acid was found in the aqueous phase.

Similar results were obtained in the presence of C_3N_4-Cy-B 1-1-0.2. Even in the presence of this photocatalyst, 4-MBA was oxidized to aldehyde with 100% selectivity, and although visible light resulted in a lower conversion than UV light, selectivity to aldehyde was always 100%. Notably, as reported in Table 1, both 4-NBA and 4-OHBA were converted more significantly under visible light irradiation than UV in the presence of the latter photocatalyst. We must consider that the reaction products in a photocatalytic reaction could however remain adsorbed on the surface of the photocatalysts or be completely mineralized.

The two samples containing the highest amount of barbituric acid were less active than the others, particularly C_3N_4-Cy-B 1-1-1, which was completely inactive.

In order to compare the activity of the various samples, the initial reaction rates of the photocatalytic benzyl alcohols conversion and benzaldehydes formation

Table 1 Conversion (X) of the benzyl alcohols and selectivity (S) percentages towards the corresponding aldehyde after 4 h of irradiation in the presence of the various photocatalysts tested using UV or LED (Vis) irradiation

Substrate	Irradiation set-up	BA		4-MBA		4-NBA		4-OHBA	
		X	S_{BAL}	X	$S_{4\text{-MBAL}}$	X	$S_{4\text{-NBA}}$	X	$S_{4\text{-OHBAL}}$
$g\text{-}C_3N_4$	UV	10	100	48	75	12	100	20	4
	Vis	5	100	48	65	9	100	32	6
C_3N_4-Cy 1-1-0	UV	29	100	100	51[(a)]	22	100	31	12
	Vis	10	100	100	93[(b)]	20	100	38	9
C_3N_4-Cy-B 1-1-0.2	UV	6	100	72	100	2	100	16	11
	Vis	5	100	57	100	4	100	23	10
C_3N_4-Cy-B 1-1-0.5	UV	Negl	Negl	42	90	Negl	Negl	6	8
	Vis	Negl	Negl	12	100	Negl	Negl	21	6
C_3N_4-Cy-B 1-1-1	UV	Negl	Negl	Negl	Negl	Negl	Negl	Negl	Negl
	Vis	Negl	Negl	Negl	Negl	Negl	Negl	Negl	Negl

(a) After 120 min of reaction, the conversion was 100% and also the selectivity reached 100% (see Fig. 8 for 4-MBAL)

(b)After 210 min of reaction, both conversion and selectivity were 100% (see Fig. 10 for 4-MBAL)

Negl. stands for negligible

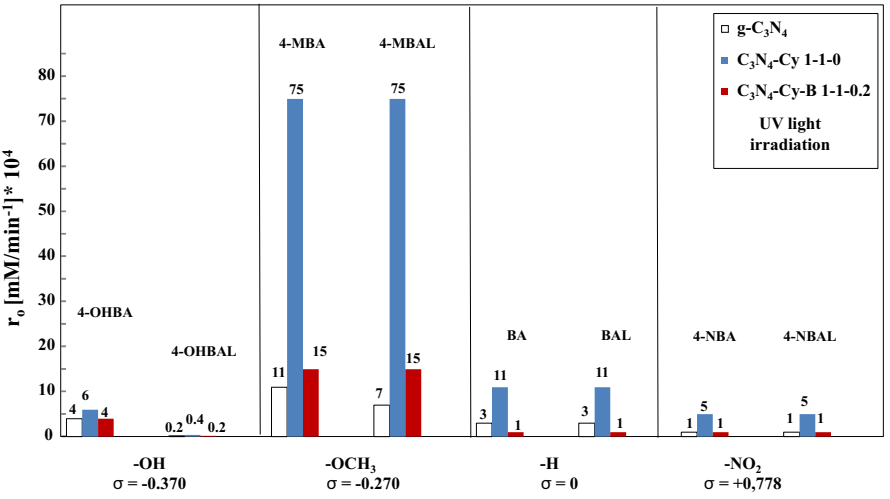

Fig. 11 Initial reaction rates for all the four benzyl alcohols oxidation and corresponding benzaldehyde formation under UV irradiation in the presence of the more active photocatalysts

were estimated by the best linear fitting experimental concentration vs. irradiation time, considering the initial stages of the reaction and consequently the results are reported as initial reaction rates. The values obtained under UV irradiation are reported in Fig. 11, where the substrates used are shown in abscises and ordered

by considering the Hammett constant (σ) of the substituent in para-position with respect to the benzyl alcohol group. It is useful to remember that the Hammett constant (σ) is a chemical parameter that quantifies the influence of a substituent on the reactivity of a molecule with respect to the basic structure in relation to the inductive and resonance effects due to the substituent. Electron-donating groups, such as –OH or $–OCH_3$, show negative Hammett constants, while electron-withdrawing groups, such as $–NO_2$, have positive Hammett constants. A relation between the Hammett constants and the photocatalytic initial rates of alcohols oxidation and aldehyde formation was considered before in the literature [56]. It has been reported that for benzyl alcohols, electron-donating substituents in *para*-position with respect to the CH_2OH-group promote the reactivity of the substrate without compromising the selectivity towards benzaldehydes if compared with the unsubstituted molecule [18].

As shown in Fig. 11, the initial reaction rate of benzyl alcohols oxidation decreases in the series 4-MBA > BA > 4-NBA. A larger Hammett constant is related to a lower reactivity of the aromatic ring, and this finding is valid both for the oxidation of alcohol and for the production of benzaldehyde. The reactivity here reported for the benzyl alcohols is in good agreement with that observed by other researchers who studied the same reaction by using different photocatalysts as TiO_2 [57–59], $BiFeO_3$/carbon nanotubes [60] or C_3N_4 as before mentioned. It should be noticed, however, that the results are not consistent with the Hammett constant of 4-OHBA, since, due to the value associated with this molecule which is the smallest among those of the substrates studied, high reactivity should be expected. Notably, Yurdakal et al. found results for the 4-OHBA molecule similar to those reported in this paper, i.e. a lower reactivity of this substrate in the reactivity sequence of various substituted benzyl alcohols, although the photocatalyst used had been in those experiments TiO_2 [57].

The mechanism of the photocatalytic benzyl alcohol oxidation can explain the above finding. The photocatalytic oxidation of benzyl alcohol in aqueous medium occurs by adsorption of the molecule on the surface of the semiconductor. According to the literature, in order to obtain the selective partial oxidation of the alcoholic group, the interaction of the aromatic substrate with the surface of the photocatalyst should take place through the alcoholic group, and the aromatic ring should not be involved in the adsorption [57, 58]. On the contrary, the total oxidation would require the interaction of the aromatic ring with the surface [57–62]. The low activity of the 4-OHBA substrate as regards the oxidation of its alcoholic group has been attributed to the interaction of this molecule with the surface of the photocatalyst by means of its hydroxyl group instead of the benzyl group.

In the presence of other electron donor groups, such as $–OCH_3$, both the reaction speed and the selectivity increase. Yurdakal et al. also observed that in the presence of TiO_2, selectivity values for the partial oxidation of 4-OHBA are similar to those obtained for BA but much lower than those obtained for 4-MBA.

In the presence of other electron-donating groups, such as the $–OCH_3$ one, both reaction rate and selectivity increase. Yurdakal et al. observed also in the presence of TiO_2 that the selectivity values for 4-OHBA partial oxidation were similar to those

obtained with BA but much lower than those obtained for 4-MBA. The adsorption of 4-MBA by means of the alcoholic group on the surface of the photocatalyst and the inductive and delocalization effects caused by the $–OCH_3$ group on the aromatic ring hinder the strong oxidizing attacks that can cause the mineralization of the molecule [57].

It cannot be excluded a possible reaction of 4-OHBA with the basic sites on the photocatalyst resulting in the inactivation or partial poisoning of the C_3N_4 photocatalyst. This behaviour has been previously observed for acidic heteropolyacids which inactivate the C_3N_4 surface by an acid–base reaction [63]. Further research is underway to investigate the possible inactivation of C_3N_4 by reaction with acid substrates.

The initial reaction rate for benzaldehyde formation for each substrate was always higher in the presence of the C_3N_4-Cy 1-1-0 sample, followed by the C_3N_4-Cy-B 1-1-0.2 and the g-C_3N_4 ones. The values of the initial reaction rate for benzaldehyde formation followed the same trend than for the benzyl alcohol oxidation and, remarkably, present very similar values, with the exception of the 4-OHBA. This can be explained by taking into account the different adsorption of 4-OHBA on the surface of the photocatalysts, as explained above.

The initial reaction rates for the benzyl alcohols oxidation and benzaldehydes formation under visible irradiation are reported in Fig. 12. The figures are similar to those shown in Fig. 11, with the exception of the most oxidizable substrate, 4-MBA, which halved the initial reaction rate. Also, in this case, the oxidation of benzyl alcohol and the formation of benzaldehyde showed very close values. These results along with those reported in Table 1 indicate that the use of the visible light irradiation is suitable for the partial oxidation of some benzyl alcohols to aldehydes.

According to the literature, we assume that the oxidation reaction of benzyl alcohols proceeds by the mechanism discussed in the following. It is widely accepted, as demonstrated in previous studies [64], that superoxide radicals, $^{\cdot}O_2^-$, obtained

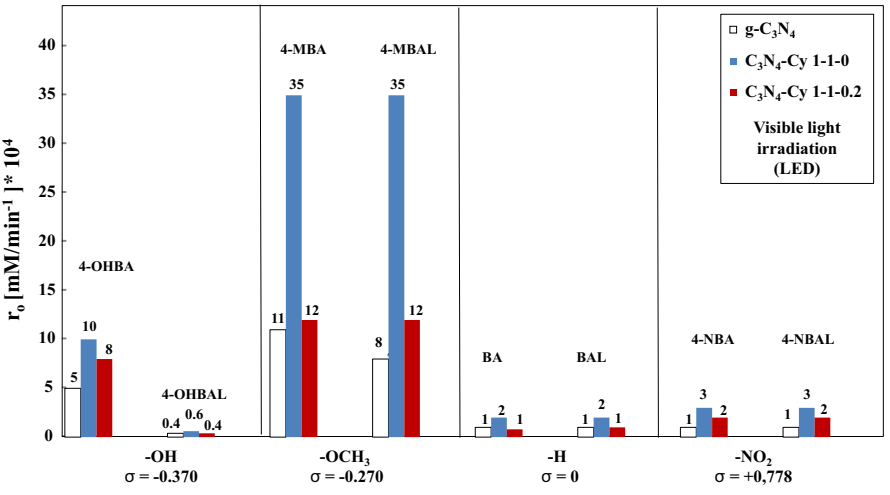

Fig. 12 Initial reaction rates for all four benzyl alcohols oxidation and benzaldehyde formation under visible irradiation in the presence of the more active photocatalysts

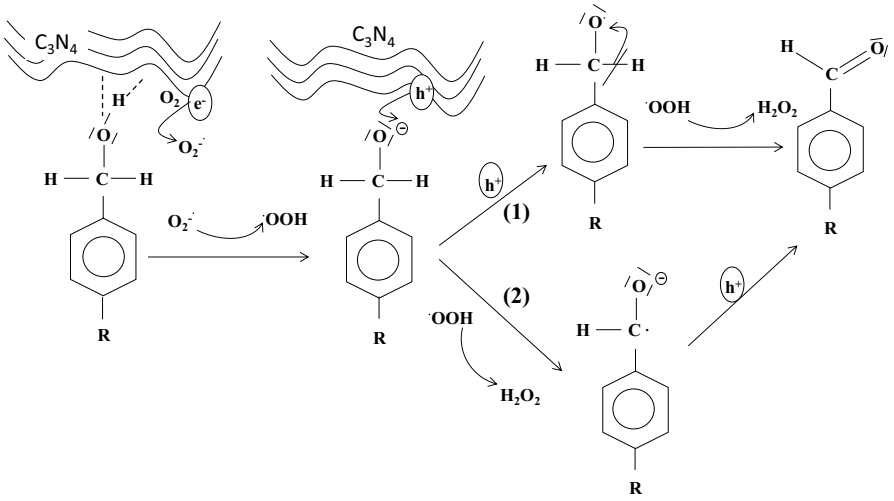

Fig. 13 Proposed pathway for the partial photocatalytic oxidation of benzyl alcohols using C_3N_4 as photocatalyst

through the reduction of molecular oxygen by photogenerated electrons act as oxidizing species (Eq. 3). This ROS (reactive oxidant species) would eventually be responsible for the partial oxidation of benzyl alcohol to aldehyde in water.

$$O_2 + e^- \rightarrow \cdot O_2^- \tag{4}$$

In Fig. 13, some essential steps of the reaction path are illustrated, in agreement with the mechanism proposed before by Antonietti et al. [14]. The superoxide species formed by the photogenerated electrons on the C_3N_4 surface deprotonates the adsorbed alcohol forming an alkoxide. We have mentioned before that the benzyl alcohol must be adsorbed by the alcoholic group on the surface of C_3N_4. The $–CH_2OH$ group would be destabilized by the interaction with the surface. The produced adsorbed alkoxide species could follow an oxidative route by following two possible pathways, indicated as (1) and (2) in Fig. 13. In path (1), the adsorbed benzyl alkoxide reacts directly with the photoproducted h^+, as suggested by Antonietti [14, 37], giving rise to a carbon radical which evolves to the aldehyde by transferring a hydrogen to the $HOO^·$ species formed via O_2. Path (2), on the other hand, first involves the reaction of the alkoxide with the $HOO^·$ species and then with the hole.

During the photocatalytic experiments, the formation of H_2O_2 was monitored. It is well known the ability of C_3N_4 to form H_2O_2 during the photocatalytic process in aqueous suspension [14, 64, 65]. Figure 14 shows its concentration in suspension using 4-MBA as the substrate both under UV and visible irradiation. It is worth remembering that H_2O_2 formed can also be decomposed by absorbing UV light (~400 nm) [66], and this is probably the reason why the amount is much lower than that of 4-MBAL reported for the same tests (Figs. 8, 10). It should be considered, moreover, that H_2O_2 is not a reaction but a transient

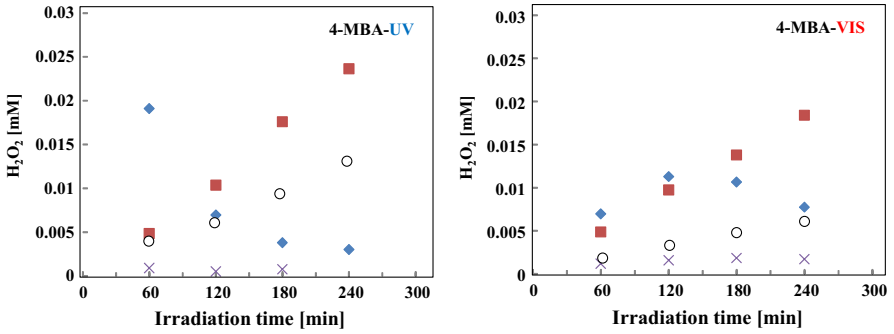

Fig. 14 H_2O_2 concentration analysed during the photocatalytic experiments versus irradiation time for runs carried out by using all the photocatalysts in the presence of UV or visible irradiation and using as substrate 4-methoxybenzyl alcohol. Initial substrate concentration: 0.5 mM in water; loading of photocatalysts: 0.33 g L^{-1}; natural pH. The values reported are the average of two runs

product. In fact, it is produced but it quickly decomposes particularly under UV irradiation into OH radicals that furtherly attack the substrate. We can assume that under UV irradiation the formation of H_2O_2 would be greater but also its decomposition is faster and more efficient forming higher amount of OH radicals. Consequently, the quantity of H_2O_2 measured in solution in both the UV and visible systems can be considered of the same order of magnitude.

The most active photocatalyst, C_3N_4-Cy 1-1-0, produced the greatest amount of H_2O_2 which, however, is subsequently likely decomposed to a large extent. In the presence of C_3N_4-Cy-B 1-1-0.2 and g-C_3N_4, lower amounts were found which increased throughout the photocatalytic experiment. The amount of H_2O_2 formed was always lower in the presence of visible light than in UV light.

Conclusions

The selective photocatalytic oxidation of four aromatic alcohols to their corresponding aldehydes has been investigated in water suspension under UV and visible irradiation by using as heterogeneous photocatalysts a set of C_3N_4 samples prepared by melamine, cyanuric acid and barbituric acid as the precursors. The presence of cyanuric acid slightly modified the C_3N_4 structure with respect to that obtained by using just melamine. By increasing the amount of barbituric acid in the preparation, both a decreasing of the order of the structure and the ability of light to activate the material were observed, and consequently, the photocatalysts showed to be less active. Also, the type of the substituents in the para-position of the aromatic alcohol substrate strongly influenced conversion and selectivity of the reaction, being the presence of the electron-releasing group (–OCH_3) the most beneficial for the reactivity. The most active material was prepared in the presence of melamine and cyanuric acid, showing a complete conversion of 4-methoxybenzyl alcohol with a 100% selectivity towards

the aldehyde even under visible irradiation, so opening the possibility to use this material for selective oxidations under solar conditions.

Memory with Prof. Michel Che

I had the privilege of meeting for the first time Prof. Che in Torino at the Congress to celebrate the retirement of Professor Coluccia; after that, I have met him a couple of times in Krakow and in Beijing four years ago. I did not have the fortune to work with him but we did speak about research and he was always very stimulating, enthusiast and kind. I remember that after our talk about heteropolyacids very informally, during social dinner in Torino, he was so kind to send me, by returning to Paris, one of his classical papers in the field. I felt so surprised that such a very important Professor, himself, he was sending to me and to Professor Palmisano a paper to enrich our work and knowledge. I was very touched and grateful. On my side and also on behalf of all the authors of this manuscript, we thank you Professor Che; you were an outstanding researcher but also a nice person. Your memory continues to inspire us.

Funding Open access funding provided by Università degli Studi di Palermo within the CRUI-CARE Agreement.

References

1. D. Friedmann, A. Hakki, H. Kim, W. Choi, D. Bahnemann, Green Chem. **18**, 5391 (2016)
2. T. Mallat, A. Baiker, Oxidation of alcohols with molecular oxygen on solid catalysts. Chem. Rev. **104**, 3037 (2004)
3. E.I. García-López, G. Marcì, M. Bellardita, L. Palmisano in developments in photocatalysis and photocatalytic Materials, ed. by Y. Wang, M. Anpo, X. Fu (Elsevier, Amsterdam, 2019), p. 437
4. S. Samanta, S. Khilari, D. Pradhan, R. Srivastava, ACS Sustain. Chem. Eng. **5**, 2562 (2017)
5. J. Kou, C. Lu, J. Wang, Y. Chen, Z. Xu, R.S. Varma R.S. , Chem. Rev. **117**, 1445 (2017)
6. F. Parrino, M. Bellardita, E.I. García-López, G. Marcì, V. Loddo, L. Palmisano, ACS Catal. **8**, 11191 (2018)
7. L. Palmisano, V. Augugliaro, M. Bellardita, A. Di Paola, E.I. García-López, V. Loddo, G. Marcì, G. Palmisano, S. Yurdakal, Chem Sus Chem **4**, 1431 (2011)
8. J.C. Colmenares, W. Ouyang, M. Ojeda, E. Kuna, O. Chernyayeva, D. Lisovytskiy, S. De, R. Luque, A.M. Balu, Appl. Catal. B **183**, 107 (2016)
9. C.J. Li, G.R. Xu, B. Zhang, J.R. Gong, Appl Catal B **115–116**, 201 (2012)
10. M. Qamar, M.O. Fawakhiry, A.M. Azad, M.I. Ahmed, A. Khan, T.A. Saleh, RSC Adv. **6**, 71108 (2016)
11. C. Zheng, G. He, X. Xiao, M. Lu, H. Zhong, X. Zuo, J. Nan, Appl. Catal. B **205**, 201 (2017)

12. X. Wang, K. Maeda, A. Thomas, K. Takanabe, G. Xin, J.M. Carlsson, K. Domen, M. Antonietti, Nat. Mater. **8**, 76 (2008)
13. P. Liu, N. Sun, Y. Liang, F. Chen, Res. Chem. Interm. **44**, 843 (2018)
14. F. Su, S.C. Mathew, G. Lipner, X. Fu, M. Antonietti, S. Blechert, X. Wang, JACS **132**, 16299 (2010)
15. B. Long, Z. Ding, X. Wang, Chem Sus Chem **6**, 2074 (2013)
16. I. Krivtsov, E.I. García-López, G. Marcì, L. Palmisano, Z. Amghouz, J.R. García, E. Díaz, S. Ordóñez, Appl Catal B **204**, 430 (2017)
17. A. Akhundi, E.I. García-López, G. Marcì, A. Habibi-Yangjeh, L. Palmisano, Res. Chem. Interm. **43**, 5153 (2017)
18. I. Krivtsov, M. Ilkaeva, E.I. García-López, G. Marcì, L. Palmisano, E. Bartashevich, E. Grigoreva, K. Matveeva, E. Díaz, S. Ordóñez, Chem. Cat. Chem. **11**, 2713 (2019)
19. M. Ilkaeva, I. Krivtsov, E.I. García-López, G. Marcì, O. Khainakova, J.R. García, L. Palmisano, E. Díaz, S. Ordóñez, J. Catal. **359**, 212S (2018)
20. M. Ilkaeva, I. Krivtsov, J.R. García, E. Díaz, S. Ordóñez, E.I. García-López, G. Marcì, L. Palmisano, M.I. Maldonado, S. Malato, Catal. Today **315**, 138 (2018)
21. M. Bellardita, E.I. García-López, G. Marcì, I. Krivtsov, J.R. García, L. Palmisano, Appl. Catal. B **220**, 222 (2018)
22. M.J. Lima, M.J. Sampaio, C.G. Silva, A.M.T. Silva, J.L. Faria, Catal. Today **328**, 293 (2019)
23. G. Palmisano, E.I. García-López, G. Marcì, V. Loddo, S. Yurkadal, V. Augugliaro, L. Palmisano, Chem. Commun. **46**, 7074 (2010)
24. C. Gomes-Silva, J.L. Faria, Chem Sus. Chem. **3**, 609 (2010)
25. L.P. Hammett, *Physical Organic Chemistry* (McGraw-Hill, New York, 1970).
26. F. Mazille, T. Schoettl, A. López, C. Pulgarin, J. Photochem, Photobiol. A **210**, 193 (2010)
27. M. Tian, S.S. Thind, M. Simko, F. Gao, A. Chen, J. Phys. Chem. A **116**, 2927 (2012)
28. S. Kitano, A. Tanaka, K. Hashimoto, H. Kominami, Phys Chem Chem Phys. **16**, 12554 (2014)
29. W.J. Ong, L.L. Tan, Y.H. Ng, S.T. Yong, S.P. Chai, Chem. Rev. **116**, 7159 (2016)
30. S. Liu, C. Liu, W. Wang, B. Cheng, J. Yu, Nanoscale **4**, 3193 (2012)
31. H. Yu, W. Zhong, X. Huang, P. Wang, J. Yu, A.C.S. Sustain, Chem. Eng. **6**, 5513 (2018)
32. H. Li, L. Wang, Y. Liu, J. Lei, J. Zhang, Res. Chem. Intermed. **42**, 3979 (2016)
33. H. Tan, X. Gu, P. Kong, Z. Lian, B. Li, Z. Zheng, Appl. Catal. B **242**, 67 (2019)
34. M. Shalom, M. Guttentag, C. Fettkenhauer, S. Inal, D. Neher, A. Llobet, M. Antonietti, Chem. Mater. **26**, 5812 (2014)
35. Y.S. Jun, E.Z. Lee, X. Wang, W.H. Hong, G.D. Stucky, A. Thomas, Adv. Funct. Mater. **23**, 3661 (2013)
36. J. Zhang, X. Chen, K. Takanabe, K. Maeda, K. Domen, J.D. Epping, X. Fu, M. Antonietti, X. Wang, Angew. Chem. Int. Ed. **49**, 441 (2009)
37. N. Keshavarzi, S. Cao, M. Antonietti, Adv. Mater. **32**, 1907702 (2020)
38. X. Li, C. Ding, C. Zhao, F. Wang, C. Li, X. Yang, Appl. Surf. Sci. **525**, 146444 (2020)
39. H. Dong, X. Guo, Y. Yin, Res. Chem. Intermed. **44**, 3151 (2018)
40. S. Kumar, N.L. Reddy, A. Kumar, M.V. Shankar, V. Krishnan, Int. J. Hydrog. Energy **43**, 3988 (2018)
41. V.N. Khabashesku, J.L. Zimmerman, J.L. Margrave, Chem. Mater. **12**, 3264 (2000)
42. J.L. Zimmerman, R. Williams, V.N. Khabashesku, J.L. Margrave, Nanoletters. Nano Lett. **1**, 731 (2001)
43. Q.H. Liang, Z. Li, X.L. Yu, Z.H. Huang, F.Y. Kang, Q.H. Yang, Adv. Mater. **27**, 4634 (2015)
44. Z.C. Yang, J. Li, F.X. Cheng, Z. Chen, X.P. Dong, J. Alloys Comp. **634**, 215 (2015)
45. Y.J. Sun, W.D. Zhang, T. Xiong, Z.W. Zhao, F. Dong, R.Q. Wang, W.K. Ho, J. Colloid Interf. Sci. **418**, 317 (2014)
46. L. Cui, J. Song, A.F. McGuire, S. Kang, X. Fang, J. Wang, C. Yin, X. Li, Y. Wang, B. Cui, ACS Nano **12**, 5551 (2018)
47. W. Tang, Y. Tian, B.W. Chen, Y. Xu, B. Li, X. Jing, J. Zhang, S. Xu, A.C.S. Appl, Mater. Interfaces **12**, 6396–6406 (2020)
48. S.C. Yan, Z.S. Li, Z.G. Zou, Langmuir **25**, 10397 (2009)
49. X.J. Bai, L. Wang, Y.J. Wang, W.Q. Yao, Y.F. Zhu, Appl. Catal. B **152–153**, 262 (2014)
50. S.F. Chen, Y.F. Hu, S.G. Meng, X.L. Fu, Appl. Catal. B **150–151**, 564 (2014)
51. Y.J. Zhang, A. Thomas, M. Antonietti, X.C. Wang, J. Am. Chem. Soc. **131**, 50 (2008)
52. J. Tauc, Mater. Res. Bull. **5**, 721 (1970)
53. F. Di Franco, A. Zaffora, M. Santamaria, Electrochim. Acta **265**, 326 (2018)
54. G. Marcì, E.I. García-López, F.R. Pomilla, L. Palmisano, A. Zaffora, M. Santamaria, I. Krivtsov, M. Ilkaeva, Z. Barbieriková, V. Brezová, Catal. Today **328**, 21 (2019)
55. Z. Sun, F. Yuan, X. Li, C. Li, J. Xu, B. Wang, Minerals **8**, 437 (2018)

56. A. Tanaka, K. Hashimoto, H. Kominami, J. Am. Chem. Soc. **134**, 14526 (2012)
57. S. Yurdakal, V. Augugliaro, RSC Adv. **2**, 8375 (2012)
58. S. Higashimoto, N. Kitao, N. Yoshida, T. Sakura, M. Azuma, H. Ohue, Y. Sakata, J. Catal. **266**, 279 (2009)
59. S. Kitano, A. Tanaka, K. Hashimoto, H. Kominami, Phys. Chem. Chem. **P16**, 12554 (2014)
60. W. Guo, Z. Zhang, H. Lin, L. Cai, Mol. Catal. **492**, 111011 (2020)
61. R. Marotta, D. Spasiano, I. Di Somma, R. Andreozzi, V. Caprio, Chem. Eng. J. **209**, 69 (2012)
62. W. Feng, G. Wu, L. Li, N. Guan, Green Chem. **13**, 3265 (2011)
63. F.R. Pomilla, F. Fazlali, E.I. García-López, G. Marcì, A.R. Mahjoub, I. Krivtsov, L.F. Liotta, L. Palmisano, Mater. Sci. Semicond. Process. **112**, 104987 (2020)
64. E.I. García-López, G. Marcì, L. Palmisano, Catal. Today **315**, 126 (2018)
65. Y. Peng, L. Zhou, L. Wang, J. Lei, Y. Liu, S. Daniele, J. Zhang, Res. Chem. Interm. **45**, 5907 (2019)
66. S. Goldstein, D. Aschengrau, Y. Diamant, J. Rabani, Environ. Sci. Technol. **41**, 7486 (2007)

(Prof. E.I. García-López)

(Dr. Z. Abbasi)

(Dr. Eng. F. Di Franco)

(Prof. M. Santamaria)

(Prof. G. Marcì)

(Prof. L. Palmisano)